NSRRC - Jo 4737(2015)

RSC Advances

PAPER

View Article Online
View Journal | View Issue

Published on 20 April 2015. Downloaded by National Chiao Tung University on 12/06/2015 02:17:17.

Cite this: RSC Adv., 2015, 5, 37323

Adsorption of *p*-nitrothiophenol on mesostructured polyoxometalate–silicate–surfactant composites containing Au nanoparticles: study of surface-enhanced Raman scattering activity†

Li-Ping Wang,[a] Shan-Chi Kuo,[a] U-Ser Jeng[b] and Ying-Huang Lai*[a]

Received 18th March 2015
Accepted 16th April 2015

DOI: 10.1039/c5ra04754d

www.rsc.org/advances

In this research, we fabricate thin-film shape-ordered mesostructured polyoxometalate–silica composites containing Au nanoparticles (NP) at the air–water interface. With three-dimensional (3D), densely packed Au NPs of 2.4 nm in size in the expanded polyoxometalate–silicate–surfactant (EPSS) template, we show that impressive surface-enhanced Raman scattering (SERS) results can be measured with *p*-nitrothiophenol (*p*-NTP) adsorbed onto Au-NPs@EPSS. The mesostructured Au-NP arrays demonstrate a SERS enhancement factor of up to 2×10^7. This high level of SERS is beyond general expectations for such small Au NPs. The surface concentration allows us to estimate the adsorption isotherms of target molecules. Quantitative data for the relationship between SERS intensity and surface coverage of adsorbates on Au-NPs@EPSS provides a better understanding of the SERS activity of 3D substrates. Furthermore, we also use a Au-NPs@EPSS composite as a catalytic and analytical platform for chemical reactions performing conversions of *p*-NTP to *p*-*p*′-dimercaptoazobenzene (DMAB) with Au-NPs@EPSS. When DMAB-functionalized Au-NPs@EPSS acts as the SERS substrate, the detection sensitivity of *p*-NTP molecules increases by ~6 times compared with as-synthesized Au-NPs@EPSS.

Introduction

Mesostructured silica has been used extensively in nanocomposite-based assays for its excellent structural properties.[1–3] Some studies have attached metal nanoparticles (NP) to mesoporous silica substrates, so as to combine the advantages of each component.[4–6] Mesostructured surface-enhanced Raman scattering (SERS)-active substrates are of particular interest, as the available surface area upon which the metal colloids may be anchored is larger than the area of a flat face. Metal NPs on the mesoporous substrate enable the preconcentration of target molecules from mixtures.[4,5,7,8] More interestingly, close and well-dispersed metal particles confined within the nanochannels of the template are the key to enhancing scattering because of the hot-spot effect. In the SERS experiments, small target molecules are absorbed on diverse types of metallic structures, including NPs, nanowires, nanorods, and nanostars.[9–12] The metal surface not only induces strong adsorption through metal and target molecule interaction, but also acts as an active SERS detection platform to trace the scattering information of adsorbed reporter molecules. Lately, some studies have reported on the use of smaller molecules, such as 4-mercaptobenzoic acid, thiophenol, or 4-aminothiophenol, as reporters, owing to their distinct SERS signatures when immobilized on the metal surface of composites.[13–15] Although the aforementioned studies focused on the activity of SERS substrates, the adsorption behavior of reporter molecules has not yet been studied with these well-documented mesostructured arrays of metallic NPs.

In our previous study, we fabricated thin-film shape-ordered mesostructured polyoxometalate–silica composites containing Au nanoparticles at the air–liquid interface.[16,17] Using the anion exchange process, $AuCl_4^-$ ions were introduced in the mesostructures and further reduced to Au metals *via* the photocatalytic reactions induced by the polyoxometalate. The Au NPs exhibited a high number density of Au NP gaps of ~1 nm.[16] In this study, we propose a photocatalytic, expanded polyoxometalate–silicate–surfactant (EPSS) template, self-assembled at the air–liquid interface. We select 1,3,5-triisopropylbenzene (TiPB) for the synthesis of the swelling agent.[18,19] TiPB is solubilized in the hydrophobic core of the micelles and thus increases their diameter and volume, leading to the expanded channel size and increased channel volume of the surfactant-templated material.[23] The free-floating EPSS

[a]Department of Chemistry, Tunghai University, Taichung, 407, Taiwan. E-mail: yhlai@thu.edu.tw

[b]National Synchrotron Radiation Research Center, Hsinchu, 300, Taiwan

† Electronic supplementary information (ESI) available. See DOI: 10.1039/c5ra04754d

This journal is © The Royal Society of Chemistry 2015

Published on 20 April 2015. Downloaded by National Chiao Tung University on 12/06/2015 02:17:17.

template allows for continuous uptake of $AuCl_4^-$ ion from the solution subphase, with the photocatalyst ($PW_{12}O_{40}^{3-}$, PTA^{3-}) embedded along the silicate–surfactant nanochannels. Cycles of adsorption and PTA^{3-} site-directed reduction of the $AuCl_4^-$ ion upon UV irradiation result in near-monodisperse Au NPs homogeneously arrayed in the mesostructured silica nanochannels.[16] Scheme 1 illustrates the conceptual synthesis route for formation of patterned metallic NP arrays *via* the EPSS template. All syntheses of the EPSS template and the subsequent metallic-NP array formation can be completed at the air–liquid interface in one Teflon container. With a correspondingly high density of hot spots for SERS, the mesostructured Au NP arrays, only 2.4 nm in size, demonstrate an impressive SERS enhancement factor of up to 10^7; this high level of SERS is beyond the general expectation for such small-sized Au NPs. We further use the Au NPs in an EPSS template (hereafter denoted as Au-NPs@EPSS) as an analytic and catalytic platform for chemical reactions and perform a conversion of *p*-nitrothiophenol (*p*-NTP) to *p*-*p*′-dimercaptoazobenzene (DMAB) with Au-NPs@EPSS.

Preparation of EPSS and Au-NPs@EPSS film

Based on the reference molar ratio of H_2O/HCl/cetyltrimethylammonium bromide (CTAB)/TiPB/tetraethyl orthosilicate (TEOS)/$PW_{12}O_{40}^{3-}$ (PTA^{3-}) = $100/1.6/0.10/0.050/0.28/3.9 \times 10^{-5}$ (optimized for observation of film formation *vs.* the control parameters used), a series of sample solutions were prepared by systemically varying the TiPB concentration. The composition was used to form free-floating films of a thermodynamically favored silicatropic phase of two-dimensional (2D) hexagonal packing, as detailed in our previous reports.[16,17,20]

GISAXS measurements

To monitor the structural evolution occurring at the air–liquid interface of the sample solutions we used the BL23A GISAXS instrument installed at the National Synchrotron Radiation Research Center (NSRRC), with a 10 keV beam of 0.2 mm diameter and 0.15°-incidence angle. Following the sample preparation procedure detailed previously,[16,20] the GISAXS patterns were collected for the subsequent adsorption of $HAuCl_4$ to the EPSS film and the formation of Au-NPs@EPSS film during UV irradiation.

TEM measurements

Field-emission transmission electron microscopy (TEM) measurements were made using a JEOL JEM-2100F microscope operated at an accelerating voltage of 200 kV. Specimens were prepared by ultrasonically suspending the Au-NPs@EPSS composites in ethanol, applying them to the copper grid, and drying them in air.

XRD measurements

Powder X-ray diffraction (XRD) measurements were performed at the BL01C2 XRD end-station of the NSRRC, Taiwan, with an X-ray wavelength, λ, of 0.775 Å (16 keV).[21] Diffraction data were collected with an image plate (Mar345) placed on the *q*-axis, and calibrated using the diffractions from mixed powders of silicon and silver behenate.

SERS experiments

The SERS samples were prepared by submerging Au-NPs@EPSS composites (1.0 mg) in ethanol solutions containing different concentrations (1 mM to 50 pM, 1.0 mL) of 4-NTP for 12 h at ambient temperature. After centrifugation, the samples were dispensed on glass slide substrates for SERS measurements. The SERS spectra were obtained using a home-built micro-Raman system.[17] The samples were irradiated with a He–Ne laser system (25 LHR/P 928, CVI Melles Griot) at 632.8 nm with output power up to 35 mW, focusing on samples of diameter 1 μm using a 40×/0.65 N.A. objective lens (Plan N, Olympus). The laser exposure time was 10 s for each spectrum. We averaged the data over six spectra for improved statistics.

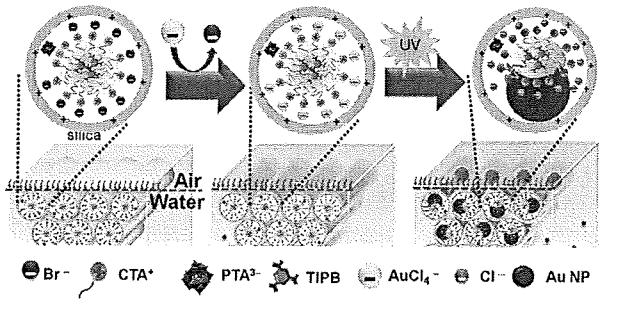

Scheme 1 Air–water synthesis route for Au-NPs@EPSS films: from the self-assembly of photocatalyst (PTA^{3-}), silica (TEOS), TiPB (swelling agent) and surfactant (CTA^+), for a EPSS film (left), followed by adsorption of metallic precursors ($AuCl_4^-$) into the EPSS film *via* anion exchange (middle), then PTA^{3-}-site-directed reduction and NP formation inside the silicate–surfactant channels upon UV irradiation, at the air–water interface (right).

Results and discussion

Process of Au-NPs@EPSS film formation

Fig. 1(a) shows a representative 2D GISAXS pattern obtained *in situ* from the air–liquid interface for a mature EPSS film (the structural evolution for the formation of the EPSS template is detailed in Fig. S1, (ESI†)). The fine reflection spots indicate a highly oriented polyoxometalate-silicatropic mesophase, formed using the expanded micelles, phase-separated to the air–liquid interface (as illustrated in Fig. 1). All the reflections can be fully indexed using 2D hexagonal (H) packing, with the (10) peak located at $q = 0.99\ nm^{-1}$ corresponding to the lattice parameter $a = 2\pi/q = 6.3$ nm. The H domain size of EPSS evaluated from the width of the (10) peak *via* the Scherrer equation is ~200 nm.[22]

Furthermore, we took GISAXS patterns with the film laterally translated over a range of ±20 mm (with the 80 mm sample dimension along the beam fully covered with an X-ray

This journal is © The Royal Society of Chemistry 2015

Published on 20 April 2015. Downloaded by National Chiao Tung University on 12/06/2015 02:17:17.

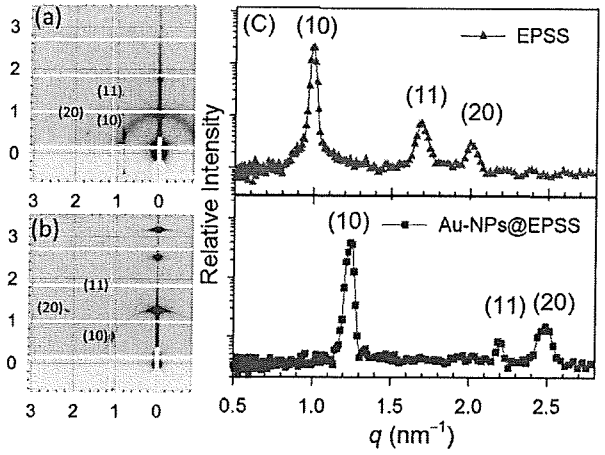

Fig. 1 GISAXS patterns observed for a self-assembled (a) EPSS film and (b) the subsequently formed Au-NPs@EPSS at the air–liquid interface upon UV irradiation. The reflections in (a) and (b) are indexed according to 2D hexagonal packing (H). (c) GISAXS profiles extracted from (a) and (b), exhibiting the positions for the first three reflections of H, as indicated. The enhanced reflection intensities for the latter case are attributed to the formation of Au NPs.

footprint). All the GISAXS patterns were similar, suggesting large-scale development of the mesostructured film comprised of highly oriented H-domains.[23] These ordered domains were, however, random in their in-plane orientation, as similar GISAXS patterns could also be observed when the sample was rotated in-plane over a range of ±10° with respect to beam incidence. After adsorption and reduction of $AuCl_4^-$ ions in the EPSS film, the *in situ* observed GISAXS patterns clearly shrunk in size (Fig. 1(b)) from those for the free-floating film of EPSS (Fig. 1(a)). The (10) peak position at $q = 0.99$ nm^{-1} shifted to 1.24 nm^{-1}. A previous report indicated that the anion in the complex charge-dipole shells of the micelles could be replaced by the $AuCl_4^-$ anion *via* anion exchange.[17,24] Reduction of the $AuCl_4^-$ anion might result in a reduced charge repulsion of the surfactant head group; this may allow free space to accommodate the Au NPs in the channels. Enhanced GISAXS peak intensities at the same facet (Fig. 1(b) and (c)) strongly suggest that the formation and ordering of the gold NPs are directed by the mesostructure of the EPSS template.[16]

The mean silica inter-channel spacing deduced from the H lattice parameter of the fully hydrated Au-NPs@EPSS composite at the air–liquid interface is 5.9 nm, which is substantially larger than that (4.2 ± 0.4 nm) determined from the TEM image (Fig. 2) for a completely dried Au-NPs@EPSS composite. The significant shrinkage by 1.7 nm in the channel spacing for the TEM sample can be attributed to the possible crumble of the lyotropic phase upon film drying. This may suggest a water-rich shell layer between the relatively hard silicate-channel wall and the soft micelles. The water-rich shell layer with the micelle counter ions provides a critical anion exchange platform and ion-pathway for $AuCl_4^-$ transportation and localization inside the silicate–surfactant channels.[16,24] In addition, the binding sites for bulky photocatalytic PTA (around 1.2 nm in size, as determined using small-angle X-ray scattering (SAXS), Fig. S2†) to the surfactant anions may become pores in the walls of the silica channels, leading to additional cross-channel diffusion of $AuCl_4^-$ for more efficient adsorption of the gold precursors into the channels.

Structure of Au-NPs@EPSS

Fig. 2(a) shows a TEM image of an Au-NPs@EPSS film exhibiting highly oriented channels of densely populated Au NPs. From the image, a mean size of ~2.4 ± 0.4 nm was determined for these Au NPs (consistent with the X-ray results shown below). Furthermore, the statistical NP spacing along the silicate nanochannels is 4.0 ± 1.1 nm (as illustrated in Fig. 2(b)), whereas the mean inter-channel spacing of the Au NP arrays (center-to-center) is 4.2 ± 0.4 nm (Fig. 2(c)). After subtracting the NP size, the gaps between NPs are determined to be 1.6 nm along the NP arrays and 1.8 nm between adjacent arrays.

Fig. 3 illustrates SERS spectra recorded from Au-NPs@PSS (without TiPB) and Au-NPs@EPSS films in the absence of analytes applied to the substrates. The SERS spectrum of Au-NPs@PSS clearly shows several strong peaks at 760, 910, 990, 1006, 1083, 1302 and 1448 cm^{-1} that are the characteristic Raman bands of CTAB (Fig. 3(a)).[25] From the spectrum (Fig. 3(b)), there is no doubt that the bands at 634, 881, 1001, 1269, and 1601 cm^{-1} are present, indicating that additional peaks could have a contribution from TiPB (a swelling agent). This observation indicates that the micelle expander is solubilized in the micelles and thus increases their diameter and volume.

Fig. S3† shows the UV-visible absorption spectra measured for a $AuCl_4^-$-adsorbed EPSS film. The adsorption band appearing at 320 nm for the composite signified the formation of $AuCl_4^-$–CTA^+ complexes.[17,26] After 3 h of UV irradiation, the 320 nm adsorption band decreased, which indicates that most of the Au atoms were generated by oxidation–reduction reactions between $AuCl_4^-$ and isopropanol through the photocatalytic agent during irradiation. X-ray energy-dispersive spectroscopy (EDS), coupled with TEM, showed that both gold and silicon elements exist throughout the Au-NPs@EPSS composite (Fig. S4†). XRD results for the Au-NPs@EPSS composition (Fig. S5†) exhibited several broad humps in the FCC structure of the Au NPs.[27,28] The particle size of 2.4 nm, estimated from the XRD peak widths *via* the Scherrer equation, is consistent with that given by the TEM image results. The combined results of the UV-visible adsorption, TEM, XRD, SERS, and GISAXS, suggest that a large number of crystallized NPs are homogeneously arrayed in the mesostructured Au-NPs@EPSS composite.

Raman spectra of EPSS

We systematically measured Raman spectra for the EPSS composites after soaking in solutions of 10, 1, 0.5, and 0.1 mM of *p*-NTP (Fig. 4). The observed marked growth of bands at 1343 and 1580 cm^{-1} may be assigned to the stretching vibrations of N–O and C–C, respectively, of *p*-NTP. As the concentration of *p*-NTP increases, the Raman intensities corresponding to the

Published on 20 April 2015. Downloaded by National Chiao Tung University on 12/06/2015 02:17:17.

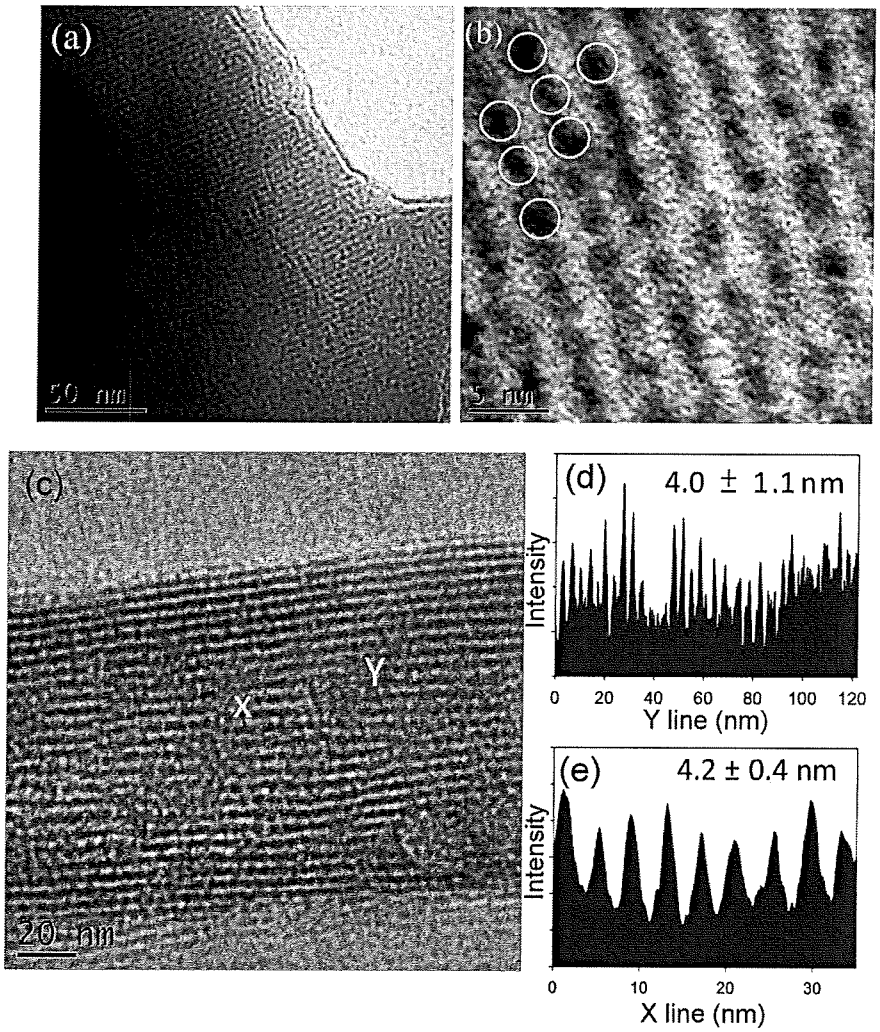

Fig. 2 (a–c) A representative TEM image of an Au-NPs@EPSS film with Au nanoparticles embedded along the nanochannels of the silicate. (d and e) Au NP location profiles along the *Y* and *X* lines marked in (c), revealing the across-channel structure with (peaks) and without (valleys) NPs.

1454 and 1486 cm^{-1} bands of CTAB become nearly identical, while those of 1343 and 1580 cm^{-1} of *p*-NTP increase. The results of the Raman spectroscopy indicate that even at a low concentration, *i.e.*, 0.1 mM, the *p*-NTP is already detectable in the EPSS composites, using the preconcentration property of the mesostructured substrate.[29] Furthermore, we should note that the Raman peaks of TiPB are difficult to observe, which suggests that most TiPB molecules are removed during SERS sample preparation.

SERS of Au-NPs@EPSS

We investigated the dependence of SERS intensities on the concentration of *p*-NTP by varying the *p*-NTP concentration for the Au-NPs@EPSS. Fig. 5 shows the SERS spectra of *p*-NTP, with two especially sharp bands clearly visible even in the case of the 50 pM *p*-NTP solution. It is known that the SERS spectrum of *p*-NTP is characterized by two especially noticeable peaks at 1337 and 1576 cm^{-1}, corresponding to the stretching vibrations of N–O and C–C, respectively.[30–32] As the concentration of *p*-NTP increases, the SERS Stokes intensities corresponding to the N–CH_3 asymmetric bending (1448 cm^{-1}) of CTAB progressively decrease, while those of the ν(N–O) and ν(C–C) band of *p*-NTP increase, indicating that the Au surface induces strong adsorption through metal and target molecule interaction. The Stokes intensities of *p*-NTP follow Langmuir's equation, $\theta = I/I_0 = \alpha[p\text{-NTP}]/(1 + \alpha[p\text{-NTP}])$, as shown in Fig. 6.[33] We compared the surface coverage (θ) to the concentration of *p*-NTP, and obtained a linear relationship from 5.0×10^{-11} M to 5.0×10^{-5} M. According to the fitted data, the average adsorption constant is 2.7×10^5. A saturated monolayer adsorption of *p*-NTP on the gold surface of Au-NPs@EPSS is achieved when the concentration of *p*-NTP is higher than 5×10^{-5} M. A higher concentration of *p*-NTP is adsorbed to the substrate through physisorption, and is located far away from the hot-spot region of scattering.

 This journal is © The Royal Society of Chemistry 2015

Published on 20 April 2015. Downloaded by National Chiao Tung University on 12/06/2015 02:17:17.

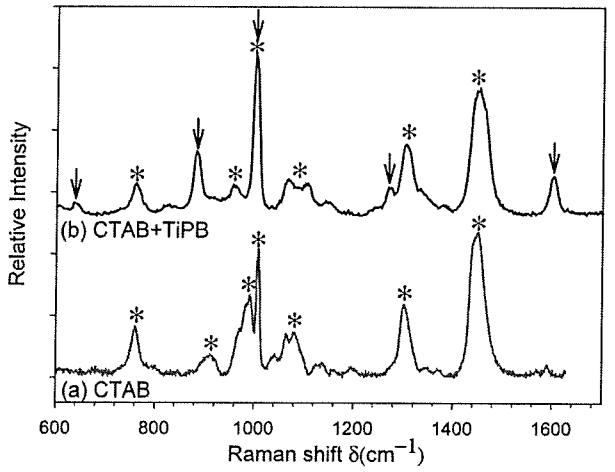

Fig. 3 SERS spectra of Au-NPs@EPSS (red) and Au-NPs@EPSS (black) substrates. The stars (*) and arrows mark the characteristic bands contributed by CTAB and TiPB, respectively. The excitation laser wavelength is 633 nm.

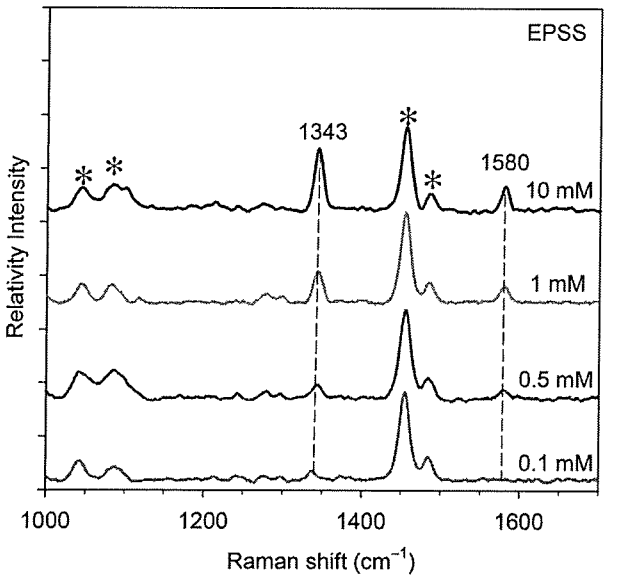

Fig. 4 Raman spectra for *p*-NTP adsorbed on EPSS composites after soaking in a solution with *p*-NTP concentrations as indicated. The stars (*) mark the characteristic bands contributed by CTAB.

Previous SERS studies[16,34] have widely discussed the enhancement effect from a quantitative point of view, and have found that the Raman cross-section undergoes a 10^4 to 10^{14}-fold enhancement in the SERS. This enhancement strongly depends on the activity of the platform, particularly on the crucial hot-spot density of SERS on the substrate. The enhancement factor (EF) of Au-NPs@EPSS for the SERS bands was calculated according to $EF = (I_S/C_S)/(I_R/C_R)$, where I_S and I_R are the corresponding band intensities of the Au-NPs@EPSS and the EPSS substrates after soaking in *p*-NTP solutions of concentrations C_S and C_R, respectively.[16,34,35] Compared to the Raman spectrum of

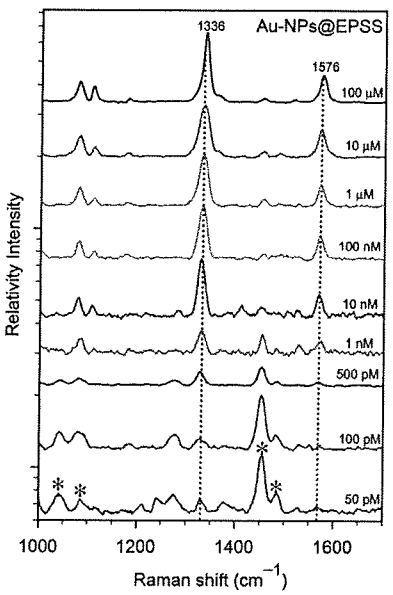

Fig. 5 SERS spectra for the Au-NPs@EPSS composites, 12 h after soaking in *p*-NTP solutions of 100, 10, and 1 μM, and 100, 10, 1, 0.5, and 0.1 and 0.05 nM of *p*-NTP.

p-NTP, adsorbed to the EPSS substrate (Fig. 4, 0.1 mM), the SERS of the Au-NPs@EPSS sample with a *p*-NTP concentration of 50 pM displays good EF values of 1.7×10^7 and 2.9×10^7, for the aforementioned 1337 and 1576 cm^{-1} bands, respectively. The SERS results demonstrated here indicate that when Au NPs are densely packed on Au-NPs@EPSS, Au NPs approximately 2.4 ± 0.4 nm in size can exhibit a significant SERS effect. The swelling agent could lead to larger Au NPs (2.4 nm), as revealed by GISAXS and TEM. As a result, the SERS spectra measured with Au-NPs@EPSS exhibited a much higher sensitivity with *p*-NTP down to 50 pM, with EF values two orders of magnitude higher than those measured using Au-NPs@PSS under a similar condition.[17] Furthermore, according to the previous study of ref. 17, the particles size of Au NPs in Au-NPs@PSS was 1.7 ± 0.2 nm. Two times higher amount of *p*-NTP can be adsorbed on Au surface of such smaller Au NPs as compared with the bigger Au NPs (around 2.4 nm) in Au-NPs@EPSS.

Our SERS results indicate that, when organized into dense arrays of 2D hexagonal packing with small NP gaps, Au NPs of a small size (around 2.4 nm) can still exhibit a significant SERS effect. We attribute the good SERS performance of the Au-NPs@EPSS composites to the three-dimension (3D) densely organized NP arrays, with respective mean NP gaps of ~1.8 and ~1.6 nm across and along the 2D hexagonally ordered Au-NP arrays. Such mesostructured Au-NP arrays have a high number density of SERS hot-spots, being proportional to the number density of the 3D closely packed Au NPs.[16]

Indeed, we could greatly improve the SERS performance of the Au-NPs@EPSS composite by converting *p*-NTP into DMAB on Au-NPs@EPSS. We soaked *p*-NTP functionalized on Au-NPs@EPSS in a 5 mM borohydride solution. The spectra shown in Fig. 7 reveal peaks at 1139 cm^{-1}, corresponding to ν(C–H),

Published on 20 April 2015. Downloaded by National Chiao Tung University on 12/06/2015 02:17:17.

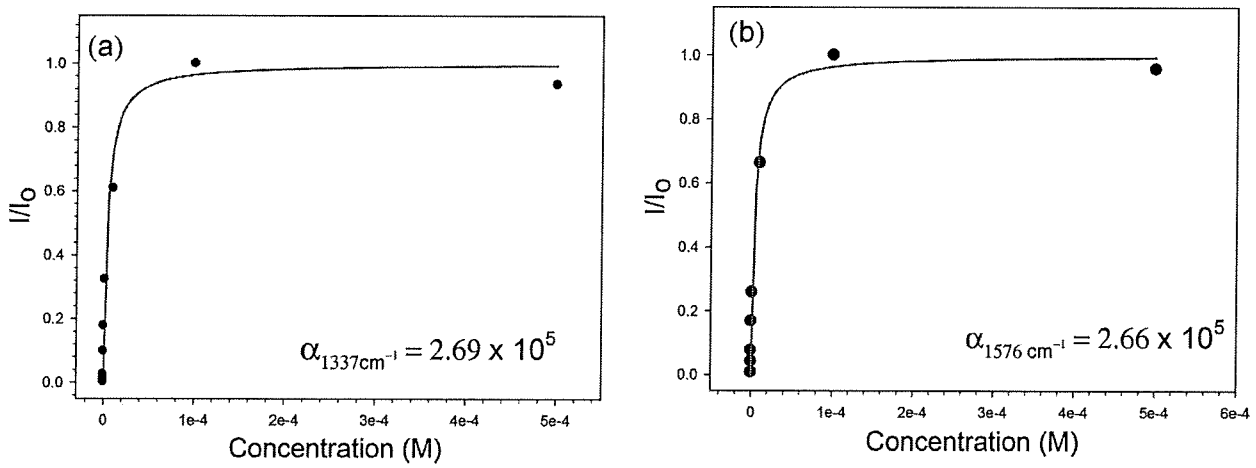

Fig. 6 Adsorption isotherms of *p*-NTP on the Au-NPs@EPSS obtained according to the (a) 1337 and (b) 1574 cm^{-1} modes in the SERS spectra.

and at 1388 and 1441 cm^{-1}, corresponding to ν(N=N), suggesting that a proportion of the *p*-NTP molecules are converted to DMAB.[31,36] Note that no additional source of *p*-NTP is supplied in the dimerization reaction and SERS experiments; as a result, the conversion of *p*-NTP into DMAB must occur as the *p*-NTP molecules have direct contact with catalyst (Au NPs). Furthermore, the formation of DMAB on Au-NPs@EPSS may result in a decrease in distance between Au NPs and/or an increase in the dielectric constant of the medium near the Au-NP surface.[37–39] These effects should simultaneously enhance the local electromagnetic field near the Au-NPs@EPSS, which significantly improves the SERS detection of *p*-NTP, as seen in Fig. 7. The integrated peak intensity (at 1336 cm^{-1}) of the *p*-NTP molecule on DMAB-functionalized Au-NPs@EPSS is 1.5–6 times higher than that on Au-NPs@EPSS.

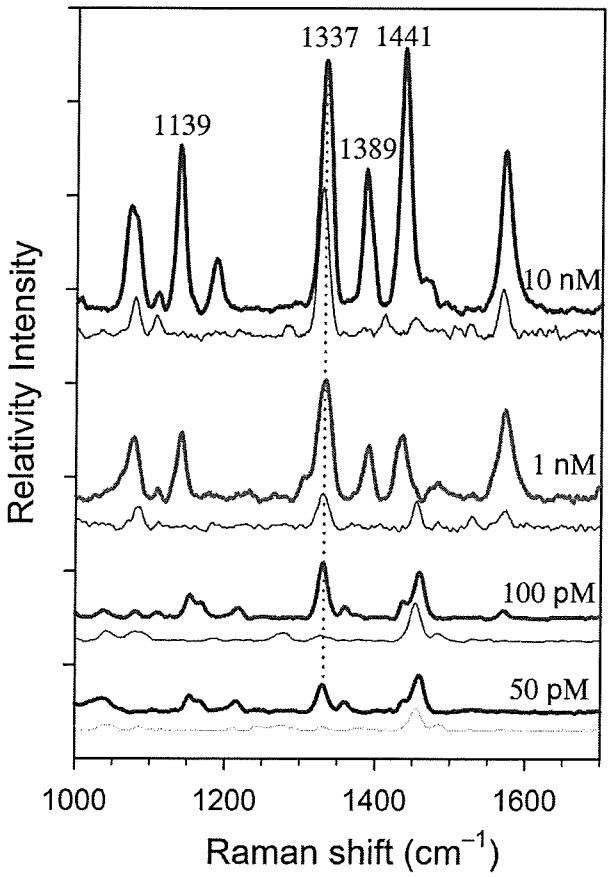

Fig. 7 SERS spectra before (fine line) and after (thick line) the catalytic reduction of *p*-NTP, functionalized on Au-NPs@EPSS by soaking in a $NaBH_4$ solution. The concentrations of *p*-NTP are 10, 1, 0.1, and 0.05 nM, respectively.

Overall, our SERS results indicate that the 3D-organized Au NPs can exhibit a significant SERS effect (EF = $\sim 2 \times 10^7$). The EPSS comprises 2D hexagonal structures that are able to absorb relatively large amounts of target molecules through chemisorption (with Au NPs) and physisorption. With NP gaps of around 2 nm across and along the hexagonally ordered Au NP arrays, the Au-NPs@EPSS film has a high density of Au NPs at $\sim 10^{19}$ NP per cm^3, resulting in a comparatively high density of SERS hot spots.

Conclusions

In this paper, we proposed a synthesis scheme for hexagonally packed arrays of densely spaced Au nanoparticles (NP) on a photocatalytic, expanded polyoxometalate–silicate–surfactant template (EPSS). *Via* a self-sustained anion exchange process activated by UV irradiation, the photocatalytic silicatropic template self-assembled at the air–liquid interface can undergo a continuous uptake of $AuCl_4^-$ anions from the solution subphase for diffusion-controlled and PTA^{3-}-site-directed photocatalytic reduction inside the silica channels. This results in homogeneously and densely distributed Au NPs of $\sim 2.4 \pm 0.4$ nm in size. The enhancement factor observed from surface-enhanced Raman scattering (SERS) rose up to $\sim 2 \times 10^7$ with 50 pM of *p*-nitrothiophenol (*p*-NTP) adsorbed on to the mesostructured Au-NPs@EPSS film. We attribute this to the very high density of SERS hot spots caused by the Au NPs.

 This journal is © The Royal Society of Chemistry 2015

Published on 20 April 2015. Downloaded by National Chiao Tung University on 12/06/2015 02:17:17.

We performed a conversion of *p*-NTP to *p*-*p*′-dimercaptoazobenzene (DMAB) with Au-NPs@EPSS to demonstrate that the Au-NPs@EPSS is capable of not only catalyzing the transformation of absorbed molecules but also sensitively monitoring the change in structure of the absorbed molecules *via* the catalyzing reduction reaction from Au NPs on the EPSS. Based on comprehensive SERS experiments, we concluded that, with narrow spacing gaps between NPs in three dimensions, the Au-NPs@EPSS composites exhibit good SERS effects. With the nanochannels in the mesostructured template, Au-NPs@EPSS can also provide a platform for studying spatially confined reactions that involve a change in the molecular structure that can be revealed using SERS.

References

1 W.-C. Huang, P.-J. Tsai and Y.-C. Chen, *Small*, 2009, **5**, 51–56.
2 J. Yao, M. Yang and Y. Duan, *Chem. Rev.*, 2014, **114**, 6130–6178.
3 C. S. Levin, J. Kundu, A. Barhoumi and N. J. Halas, *Analyst*, 2009, **134**, 1745–1750.
4 S. Xuan, Y. Zhou, H. Xu, W. Jiang, K. C.-F. Leung and X. Gong, *J. Mater. Chem.*, 2011, **21**, 15398–15404.
5 J. Ge, T. Huynh, Y. Hu and Y. Yin, *Nano Lett.*, 2008, **8**, 931–934.
6 W. Yu, Y. Huang, L. Pei, Y. Fan, X. Wang and K. Lai, *J. Nanomater.*, 2014, **2014**, 8.
7 H.-J. Cui, J.-W. Shi, B. Yuan and M.-L. Fu, *J. Mater. Chem. A*, 2013, **1**, 5902–5907.
8 H. Cong, B. Yu, J. Tang, Z. Li and X. Liu, *Chem. Soc. Rev.*, 2013, **42**, 7774–7800.
9 A. Mezni, I. Balti, A. Mlayah, N. Jouini and L. S. Smiri, *J. Phys. Chem. C*, 2013, **117**, 16166–16174.
10 A. Gole, J. W. Stone, W. R. Gemmill, H.-C. zur Loye and C. J. Murphy, *Langmuir*, 2008, **24**, 6232–6237.
11 E. Esenturk and A. Hight Walker, *J. Nanopart. Res.*, 2012, **15**, 1–10.
12 M. S. Goh, Y. H. Lee, S. Pedireddy, I. Y. Phang, W. W. Tjiu, J. M. R. Tan and X. Y. Ling, *Langmuir*, 2012, **28**, 14441–14449.
13 A. Gole, N. Agarwal, P. Nagaria, M. D. Wyatt and C. J. Murphy, *Chem. Commun.*, 2008, 6140–6142.
14 S.-Y. Han, Q.-H. Guo, M.-M. Xu, Y.-X. Yuan, L.-M. Shen, J.-L. Yao, W. Liu and R.-A. Gu, *J. Colloid Interface Sci.*, 2012, **378**, 51–57.
15 H. Hwang, S.-H. Kim and S.-M. Yang, *Lab Chip*, 2011, **11**, 87–92.
16 Y.-H. Lai, S.-W. Chen, M. Hayashi, Y.-J. Shiu, C.-C. Huang, W.-T. Chuang, C.-J. Su, H.-C. Jeng, J.-W. Chang, Y.-C. Lee, A.-C. Su, C.-Y. Mou and U. S. Jeng, *Adv. Funct. Mater.*, 2014, **24**, 2544–2552.
17 S.-C. Kuo, J.-J. Tasi, J.-S. Li, Z.-H. Hou, C.-H. Li, U.-S. Jeng and Y.-H. Lai, *APL Mater.*, 2014, **2**, 113310.
18 J. L. Ruggles, E. P. Gilbert, S. A. Holt, P. A. Reynolds and J. W. White, *Langmuir*, 2003, **19**, 793–800.
19 L. Cao, T. Man and M. Kruk, *Chem. Mater.*, 2009, **21**, 1144–1153.
20 Y.-H. Lai, S.-W. Cheng, S.-W. Chen, J.-W. Chang, C.-J. Su, A.-C. Su, H.-S. Sheu, C.-Y. Mou and U. S. Jeng, *RSC Adv.*, 2013, **3**, 3270–3283.
21 Y.-F. Song, C.-H. Chang, C.-Y. Liu, S.-H. Chang, U. S. Jeng, Y.-H. Lai, D.-G. Liu, S.-C. Chung, K.-L. Tsang, G.-C. Yin, J.-F. Lee, H.-S. Sheu, M.-T. Tang, C.-S. Hwang, Y.-K. Hwu and K. S. Liang, *J. Synchrotron Radiat.*, 2007, **14**, 320–325.
22 K. J. Edler, *Soft Matter*, 2006, **2**, 284–292.
23 T. Brennan, S. J. Roser, S. Mann and K. J. Edler, *Chem. Mater.*, 2002, **14**, 4292–4299.
24 M.-C. Liu, H.-S. Sheu and S. Cheng, *J. Am. Chem. Soc.*, 2009, **131**, 3998–4005.
25 A. Gibaud, J. F. Bardeau, M. Dutreilh-Colas, M. Bellour, V. V. Balasubramanian, A. Robert, A. Mehdi, C. Reye and R. J. Corriu, *J. Mater. Chem.*, 2004, **14**, 1854–1860.
26 V. Amendola and M. Meneghetti, *J. Phys. Chem. C*, 2009, **113**, 4277–4285.
27 C. K. Tsung, W. B. Hong, Q. H. Shi, X. S. Kou, M. H. Yeung, J. F. Wang and G. D. Stucky, *Adv. Funct. Mater.*, 2006, **16**, 2225–2230.
28 W. Yan, V. Petkov, S. M. Mahurin, S. H. Overbury and S. Dai, *Catal. Commun.*, 2005, **6**, 404–408.
29 D. Fernand, C. Pardanaud, D. Bergé-Lefranc, P. Gallice and V. Hornebecq, *J. Phys. Chem. C*, 2014, **118**, 15308–15314.
30 W. Xie, B. Walkenfort and S. Schlücker, *J. Am. Chem. Soc.*, 2012, **135**, 1657–1660.
31 X. Ren, E. Tan, X. Lang, T. You, L. Jiang, H. Zhang, P. Yin and L. Guo, *Phys. Chem. Chem. Phys.*, 2013, **15**, 14196–14201.
32 H.-Y. Wu, Y.-H. Lai, M.-S. Hsieh, S.-D. Lin, Y.-C. Li and T.-W. Lin, *Adv. Mater. Interfaces*, 2014, **1**, 1400119.
33 H. Wang, C. S. Levin and N. J. Halas, *J. Am. Chem. Soc.*, 2005, **127**, 14992–14993.
34 M. Muniz-Miranda and G. Sbrana, *J. Phys. Chem. B*, 1999, **103**, 10639–10643.
35 S. L. Kleinman, B. Sharma, M. G. Blaber, A.-I. Henry, N. Valley, R. G. Freeman, M. J. Natan, G. C. Schatz and R. P. Van Duyne, *J. Am. Chem. Soc.*, 2012, **135**, 301–308.
36 B. Dong, Y. Fang, X. Chen, H. Xu and M. Sun, *Langmuir*, 2011, **27**, 10677–10682.
37 P. K. Jain and M. A. El-Sayed, *Nano Lett.*, 2008, **8**, 4347–4352.
38 M. N. Mendis, H. S. Mandal and D. H. Waldeck, *J. Phys. Chem. C*, 2013, **117**, 25693–25703.
39 B. J. Kennedy, S. Spaeth, M. Dickey and K. T. Carron, *J. Phys. Chem. B*, 1999, **103**, 3640–3646.